



PERGAMON

Journal of Quantitative Spectroscopy &
Radiative Transfer 81 (2003) 473–485

Journal of
Quantitative
Spectroscopy &
Radiative
Transfer

www.elsevier.com/locate/jqsrt

Absorption of local thermodynamic equilibrium aluminum at different densities

F. Thais^{a,*}, S. Bastiani^b, T. Blenski^a, C. Chenais-Popovics^b, K. Eidman^c,
W. Fölsner^c, J.-C. Gauthier^b, F. Gilleron^{b,1}, M. Poirier^a

^aCEA/Saclay, DSM, F-91191 Gif-sur-Yvette Cedex, France

^bLULI, UMR no. 7605 CNRS, École Polytechnique, CEA, Université Paris VI, F-91128 Palaiseau Cedex, France

^cMax-Planck Institut für Quantenoptik, D-85748 Garching, Germany

Accepted 15 February 2003

Abstract

Increasing the range of plasma parameters accessible for laboratory absorption coefficients measurements is of interest for astrophysical applications. Aluminum is of special interest as its 1s–2p inner shell absorption transitions permit one to precisely determine the ionization balance that is strongly dependent on the electron temperature. A method to increase the density of the probed sample was tested on aluminum confined by carbon tampers of different thickness (8–70 $\mu\text{g}/\text{cm}^2$). This created a density increase in the aluminum of a factor of ~ 10 . Measurements showed that the aluminum ionization decreases substantially with increasing carbon thickness. Radiative hydrodynamic simulations showed that density and temperature gradients could not be neglected and had to be taken into account in calculating the absorption structures with the atomic physics code HULLAC. Very good agreement between theory and experiment was obtained by coupling HULLAC with hydrodynamic simulations.

© 2003 Elsevier Science Ltd. All rights reserved.

Keywords: Radiatively heated plasmas; X-ray absorption spectroscopy; Opacity codes; Radiative hydrodynamic simulations

1. Introduction: motivations for Al absorption measurements

Photo-absorption coefficients are essential for radiative transfer in hot plasmas. This is true for both local thermodynamic equilibrium (LTE) and non-LTE plasmas found, e.g., in inertial confinement fusion or astrophysics. In the latter, the radiative energy transfer is dominated by X-ray absorption

* Corresponding author.

E-mail address: frederic.thais@cea.fr (F. Thais).

¹ Present address: CEA-DAM, F91 Bruyères-le-Châtel, France.

over a very wide range of densities and temperatures, especially in the sun [1] or in galactic nuclei [2]. Further, photo-absorption is important for diagnostics of laboratory plasmas.

In recent years, a series of laboratory experiments using energetic lasers have been performed in which LTE plasma opacities were measured. Results of these measurements have been published in the literature, and reviewed recently [3]. In the opacity experiments performed previously using radiatively heated “sandwich” targets composed of thin layers of material placed between two thin layers of plastic or carbon, the plasma density was relatively low being on the order of 0.005 g/cm^3 . In experiments using future-generation high-energy lasers, it will be possible to increase the plasma density, which will be of special interest for the study of density effects.

This paper relates a series of experiments performed to test the ability to model absorption spectra in plasmas at densities higher than in previous experiments, e.g., those in which aluminum was used to provide a temperature diagnostic in a nickel opacity measurements [4]. In the present experiments, we have increased the thickness of the carbon tampers and show that the sample density can be increased by a factor of 10. This value is supported by radiation hydrodynamic (hydrocode) simulations discussed in Section 3.

The experiments presented here were performed with an aluminum sample, a low- Z material, which provides a diagnosis of the temperature. That is, the absorption structures corresponding to the aluminum $1s$ – $2p$ bound electron transitions are very sensitive to the electron temperature. The spectrum of the low- Z element can be calculated using detailed atomic physics codes such as HULLAC [5]. The positions of these transitions on the wavelength scale do not change with temperature, but their strengths determine the aluminum ion distribution from which the value of temperature can be deduced, assuming LTE conditions.

Further, we used the SCO code that takes into account plasma screening [6,7] for comparison with the HULLAC calculations that do not include this effect.

2. Experimental setup and method

Two beams of the neodymium-glass LULI laser ($0.53 \mu\text{m}$, 30 J/beam , 600 ps square shaped) were focused on 1000 \AA converter foils glued on a 1 mm diameter gold cavity (Fig. 1). The cavity was heated by the X-ray emission resulting from the laser interaction that irradiates the inside of the gold cavity. This X-ray radiation had an energy distribution similar to a Planckian spectrum with a 40 eV radiative temperature. We observed that self-emission, possibly due to the luminosity of the colliding gold foils, was negligible in our case. The sample, an Al sample tamped by C of thicknesses from 8 to $70 \mu\text{g/cm}^2$, was positioned perpendicular to the cavity symmetry axis and was thus heated from one side, see Fig. 1.

A third beam, delayed by 500 ps with respect to the two heating beams, was focused to high intensity on a samarium sample located 3 mm from the center of the cavity to produce the backlighter. Delays of 200 and 900 ps were also used. The backlighter spectrum was recorded on a shot different from the absorption spectrum, just after or before the absorption shot. The spectra were recorded with a thallium-hydrogen-phthalate (TIAP) flat crystal spectrometer with a spectral resolving power $\lambda/\Delta\lambda \sim 700$. A $7 \mu\text{m}$ thick beryllium filter was set in front of the detector and Kodak DEF film provided the recording medium. The transmission data was obtained by the ratio of a samarium spectrum absorbed by the sample and that which directly passed to the detector. As these two

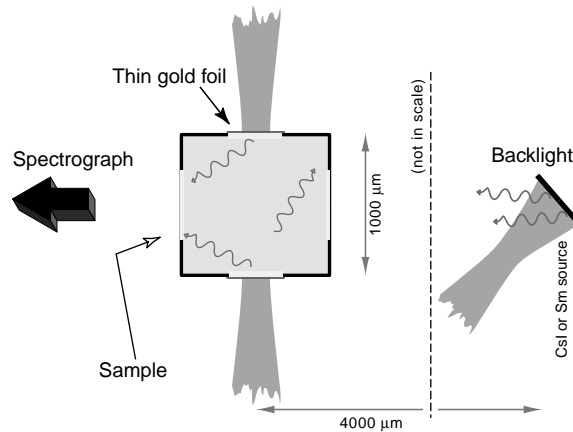


Fig. 1. Experimental setup.

spectra were not recorded on the same shot, we used an adjustment factor to superimpose the two spectra in the spectral region that contained no absorption features due to the sample. Sm backlighter spectra were wavelength-calibrated with an emission aluminum spectrum, using the He-like $1s^2-1s2p$ line, its satellites and the cold $K\alpha$ line which appears weakly on Al emission spectra.

3. Hydrodynamic simulations

Hydrocode simulations have been performed to evaluate the state of the plasma, and also as a basis of the results analysis. Although the geometry of the cavity has 3D characteristics, we could perform the computation using two 1D simulations as a first approximation. The 1D simulations were performed using MULTI, a planar 1D code solving the coupled hydrodynamic and radiation transfer equations [8]. This code uses an implicit numerical scheme with the radiative transfer treated via a multigroup model (in frequencies and angles). The laser energy deposition was treated by inverse bremsstrahlung, the electron conduction was given by the Spitzer formula, and the opacities [9] and equation of state were tabulated.

First, the X-ray emission coming from the rear-side of a 1000 \AA laser-heated gold foil was calculated. In this simulation, the laser irradiance was $5 \times 10^{13} \text{ W/cm}^2$. Then, for the X-ray heated target itself, a second simulation was run, taking into account the geometry of the energy transfer between the gold foils and the sample using a view factor of 0.12, which was adjusted to be consistent with previous experiments [10,4]. Thus, spatial and temporal variations of the density and temperature in the X-ray heated sample itself were obtained at the times of interest. During the time of the absorption measurement, the density and temperature profiles could be quite different, depending of the type of the sample, i.e., the thickness of the carbon and aluminum layers. A typical situation for the temporal evolution of the electron temperature is plotted in Fig. 2, which is the case of a $26 \mu\text{g/cm}^2$ sample of aluminum tamped by $8 \mu\text{g/cm}^2$ of carbon. The backlighting delay with respect to the main heating pulse was optimized to minimize the gradients and also ensure that the collision of the gold foils does not interfere with the measurements. Previous experiments [11] show that this

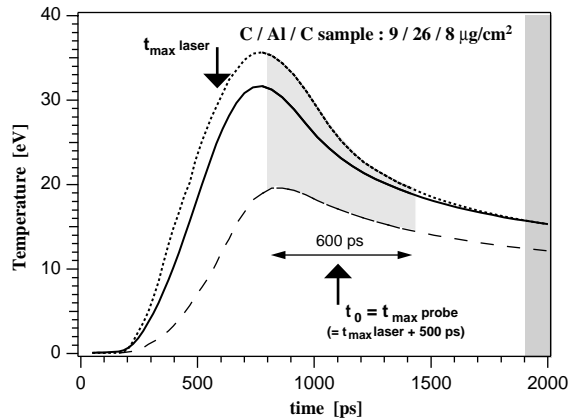


Fig. 2. Time scenario of expansion and measurement given by the MULTI simulation. The temperature is plotted as a function of the time for front (dotted line), center (plain line) and rear (dashed line) of the Al layer. The probe time shown in pale gray has the usual delay of 500 ps after the heating maximum, and the foils collision region is in dark gray.

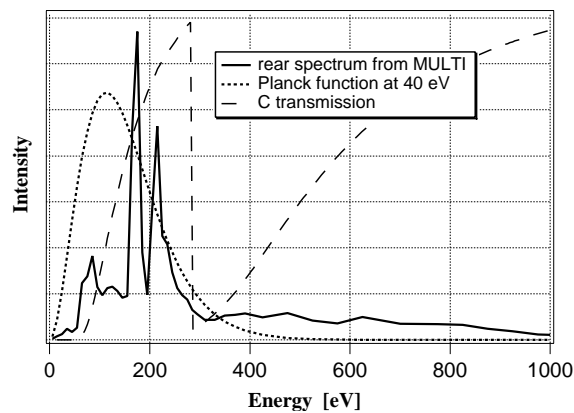


Fig. 3. X-ray spectrum emitted by the rear side of a 1000 Å gold converter foil calculated by MULTI (plain line) and compared to a 40 eV Planckian (dotted line). The C-layer transmission is plotted for a 70 μg/cm² layer (dashed line).

collision occurs at ~ 1300 ps after the laser maximum, as indicated in Fig. 2. Thus, the optimum backlighting time is between 500 and 800 ps after the laser pulse maximum, and here, the delay of 500 ps was used for most of the measurements.

It is also necessary to verify that using a thick carbon tamper to increase the density does not create a major perturbation of the heating of the aluminum layer. To determine the effect of C thickness on the Al temperature, we compare the heating spectrum with the carbon transmission. In Fig. 3, the calculated X-ray spectrum emitted by a gold converter foil is shown compared to a 40 eV Planckian spectrum and to the transmission of a 70 μg/cm² thick carbon foil. First, the Planckian and the simulated spectra are slightly different but in the same range of energy. Second, one can

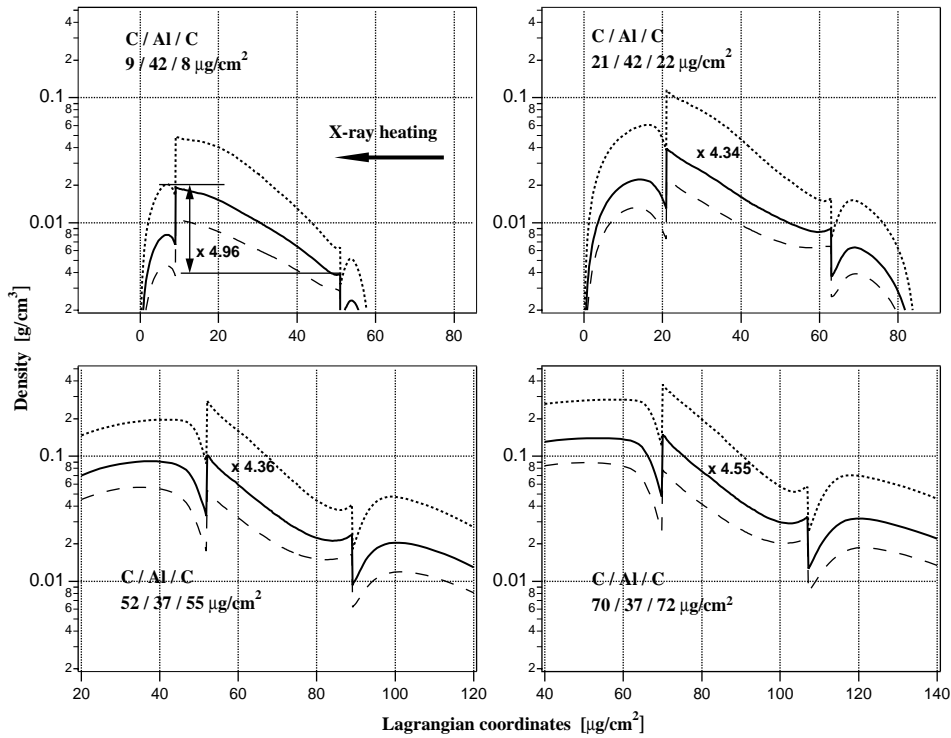


Fig. 4. Density as a function of the Lagrangian mass coordinate, calculated with the code MULTI, for a $40 \mu\text{m}/\text{cm}^2$ Al sample and the four different carbon thicknesses used in the experiment as indicated. The plain curves correspond to the measurement time t_m (500 ps after the heating pulse). The two other curves are plotted for $t_m + 300$ ps (dashed line) and $t_m - 300$ ps (dotted line).

see that the bulk of the heating spectrum is below the carbon K-edge at 400 eV. Thus, the thicker tamper only slightly modifies the heating.

In Figs. 4 and 5, the profiles of density and electron temperature are shown as a function of the lagrangian coordinates (i.e., position in the foil at initial time) given by the MULTI simulations for a $\sim 40 \mu\text{g}/\text{cm}^2$ aluminum sample and the different carbon tamper thickness used in our experiment. The solid curve is the data at the maximum of the backlighter, t_0 . The parameters are indicated for times $t_0 \pm 300$ ps, in the dashed curves, permitting estimates of the spatial and temporal gradients in the Al layer.

In Fig. 4, the effect of the C tamper thickness on the density of the sample is clearly visible. Increasing this thickness from 8 to $70 \mu\text{g}/\text{cm}^2$, the mean density varies from 10^{-2} to nearly $10^{-1} \text{g}/\text{cm}^3$. Unfortunately, the gradients are quite large, even though the ion populations do not vary very much with density. For the case of a $8 \mu\text{g}/\text{cm}^2$ tamper, the density varies by a factor of ~ 5 along the sample thickness. The gradient does not vary widely when the density increases for thicker carbon tampers, the density gradient being ~ 4.6 for the thickest tamper. Time variations of the density during the backlighter pulse are on the same order of magnitude as the spatial gradients as can be seen in Fig. 4.

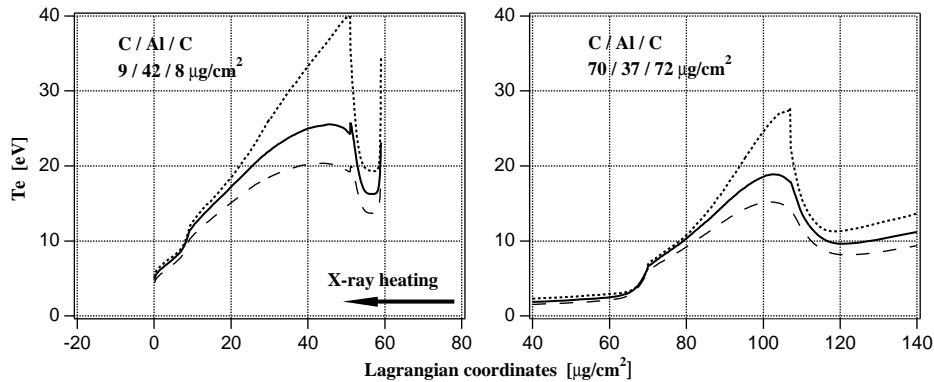


Fig. 5. Electronic temperature as a function of the Lagrangian mass coordinate, calculated with the code MULTI, for a $40 \mu\text{m}/\text{cm}^2$ Al sample and for the minimum and maximum carbon thickness, as indicated. The plain curves correspond to the measurement time t_m (500 ps after the heating pulse). The two other curves are plotted for $t_m + 300$ ps (dashed line) and $t_m - 300$ ps (dotted line).

The spatial and temporal variations of the temperature, shown in Fig. 5, are also important. Spatially, the temperature varies by about 10 eV along the Al sample thickness, and the time variation is on the same order. Further, heating is less efficient for a thick tamper as the mean temperature drops from 20 to 15 eV when the tamper thickness is increased from 8 to $70 \mu\text{g}/\text{cm}^2$. This can be due to the absorption of the high-energy component of the heating spectrum, i.e., at energies greater than 400 eV.

Due to the large density and temperature gradients, and the simultaneous change of density and temperature with the carbon tamper thickness, the experimental results will be analyzed using the profiles predicted by the hydrocode MULTI. This is in distinction with our usual procedure that consisted of fixing the density and determining a single average temperature.

4. Atomic physics calculations

In order to obtain the ion distribution in the Al plasma and its optical properties, two theoretical approaches have been used. The first one relies on the detailed atomic code HULLAC [12,13,5] based on a relativistic parametric potential. This code provides the transmission associated to each isolated ion species. In a subsequent step, the abundance of the various ions are deduced from either a Saha–Boltzmann law or by manual input, and the overall transmission is then computed. The version employed here is to calculate each individual line [12,13], as unresolved transition arrays (UTAs) are unnecessary for these low temperatures where a small number of transitions are involved for the 1s–2p absorption of aluminum. In this case, the transitions involving several electrons, which generate dielectronic satellites can be neglected. The HULLAC calculations have been used as a post-processor of the hydrocode MULTI for most of the analysis, as explained below.

Free electron screening is not accounted for in HULLAC. So, a second calculation relying on the SCO code [6,7], based on the superconfiguration description of the atomic structure [14], was used. This model accounts for LTE thermodynamics to determine the ion distribution. It includes also the screening of the nucleus due to the free electrons [15,16].

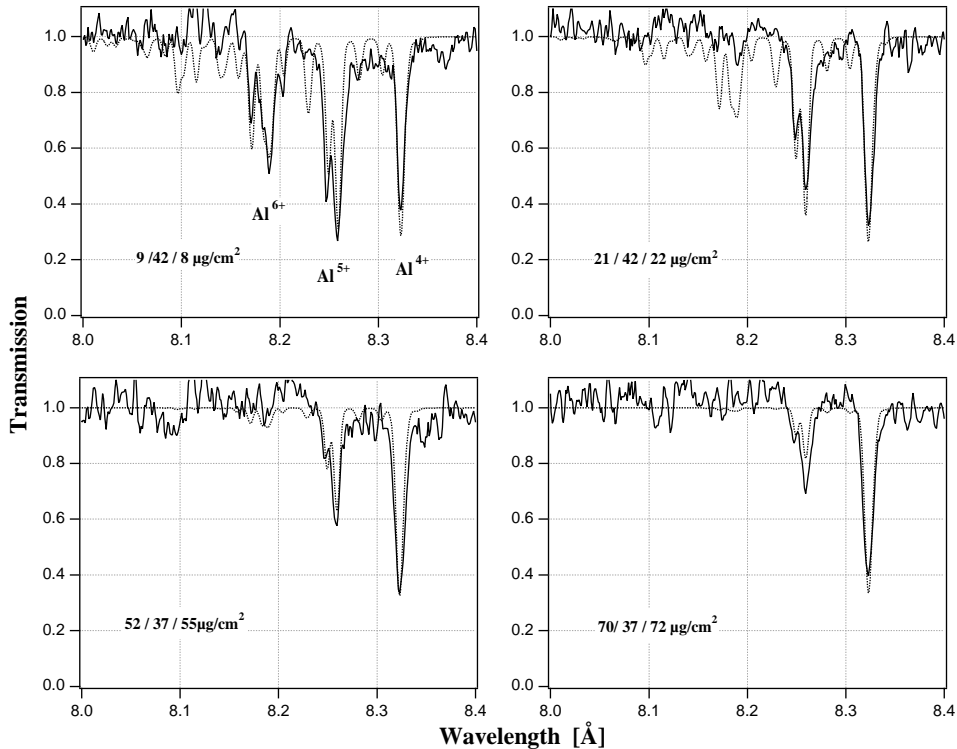


Fig. 6. Comparison of HULLAC modeling coupled with the code MULTI for, with aluminum 1s–2p transmission spectra measured for a $40 \mu\text{g}/\text{cm}^2$ Al sample and different carbon thicknesses, as indicated. The measurement is delayed by 500 ps versus the heating pulse. Plain line: experiment; dotted line: simulation.

5. Experimental results

Transmission of the 1s–2p Al transitions have been measured in the 8.1–8.35 Å range for different absorbing samples. Aluminum samples of 20 and $40 \mu\text{g}/\text{cm}^2$ thickness have been measured, for a delay of 500 ps between the heating beams and the backlighter. Data recorded for $40 \mu\text{g}/\text{cm}^2$ Al samples and for different carbon tampers (8, 20, 50 and $70 \mu\text{g}/\text{cm}^2$) are shown in Fig. 6. The ionization stays at a relatively low level. For a thin carbon tamper, one can see clearly the absorption due to Al^{4+} – Al^{6+} , as indicated in Fig. 6. The ionization decreases for increasing tamper thickness, with Al^{4+} becoming dominant for 50 and $70 \mu\text{g}/\text{cm}^2$ tamper thickness. Results obtained with a $20 \mu\text{g}/\text{cm}^2$ Al sample are very similar. For a thin tamper, transmission is as low as 0.2 for $40 \mu\text{g}/\text{cm}^2$ and 0.4 for $20 \mu\text{g}/\text{cm}^2$, indicating that we are in the linear absorption regime.

To test the effect of the backlight delay time on the absorption spectrum a few shots were performed for a fixed C tamper thickness of $50 \mu\text{g}/\text{cm}^2$ and Al sample of $40 \mu\text{g}/\text{cm}^2$, while varying the delay between the main heating X-ray pulse and the backlighter. In Fig. 7, the transmission spectra obtained for 200, 500 (as Fig. 6) and 900 ps delays are shown. It can be seen in Fig. 7 that for these conditions the ionization does not vary significantly in time.

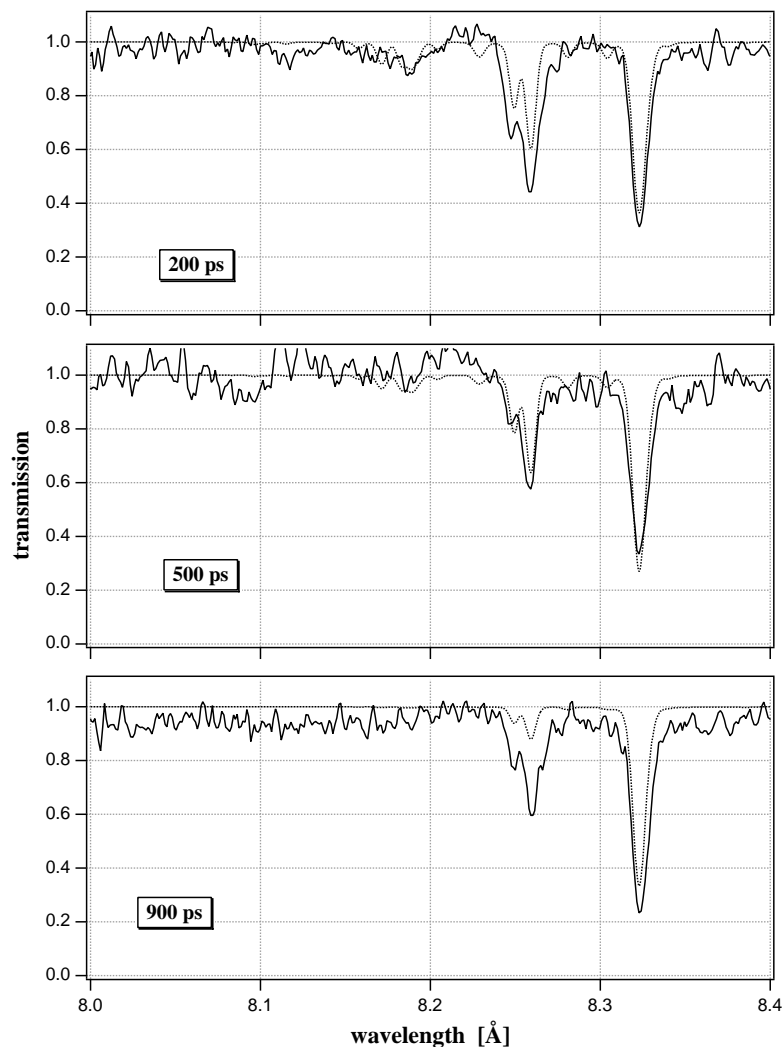


Fig. 7. Aluminum 1s–2p transmission spectra measured for a $52/37/55 \mu\text{m}/\text{cm}^2$ C/Al/C sample at different times (200, 500 and 900 ps after the heating pulse maximum). Plain line: experiment; dotted line: simulation.

A quantitative analysis of these data has been obtained by fitting the experimental data to HULLAC using manually determined ion fractions. This procedure permits one to deduce the ion fractions and the average ion charge of the measured plasma. These results, corresponding to Figs. 6 and 7, are given in Table 1. The ionization is slightly higher for the $20 \mu\text{g}/\text{cm}^2$ Al samples ($\langle Z \rangle = 3.5\text{--}4.6$) than for thicker Al samples ($\langle Z \rangle = 3.8\text{--}5.1$), but of the same order of magnitude. As a function of time, ionization does not vary significantly, the difference being under the 0.1 experimental error bar.

Table 1
Fit of the experimental transmission with ionic populations manually inserted in the HULLAC code

Target type	F-like ($Z = 4$)	O-like ($Z = 5$)	N-like ($Z = 6$)	C-like ($Z = 7$)	B-like ($Z = 8$)	$\langle Z \rangle$
40 $\mu\text{g}/\text{cm}^2$						
9/42/8	0.120	0.350	0.360	0.170	0.000	5.58
21/42/22	0.385	0.410	0.180	0.025	0.000	4.84
53/37/55	0.405	0.440	0.140	0.015	0.000	4.77
70/37/72	0.550	0.360	0.090	0.000	0.000	4.54
20 $\mu\text{g}/\text{cm}^2$						
9/26/8	0.070	0.200	0.350	0.320	0.060	6.10
21/26/22	0.100	0.320	0.400	0.150	0.030	5.69
52/20/55	0.140	0.440	0.350	0.070	0.000	5.35
70/20/72	0.330	0.520	0.150	0.000	0.000	4.82
40 $\mu\text{g}/\text{cm}^2$ fct time						
200 ps	0.265	0.490	0.210	0.035	0.000	5.02
500 ps	0.405	0.440	0.140	0.015	0.000	4.77
900 ps	0.200	0.670	0.130	0.000	0.000	4.93

6. Comparison of experimental and simulation results

Experimental results have been compared to transmission spectra calculated with HULLAC used as a post-processor of the MULTI hydrocode simulations.

First, we compared the experimental transmission spectra to HULLAC calculations performed with densities and temperatures averaged in space and time, as in previous works. In Fig. 8, the comparisons performed in this manner are plotted. Average densities and temperatures are given in the figure caption. The temperature varies from 13 to 20 eV, and accordingly, the density decreases from 0.14 to 0.024 g/cm^3 . Using these mean parameters, the theory gives an ionization that is systematically lower than experiment. This is expected from the strong temperature and density variations shown in Figs. 4 and 5.

Following these simulations, it was considered essential to fully couple HULLAC to the hydrodynamic simulations. Here we use a space and time grid that has 10×10 points. A case has been tested with a 20×20 grid of points, and no significant changes were observed. Then the total opacity of the sample was given by a product of each spatial cell contribution:

$$\tau(t_n) = \prod_i e^{-K_i \rho_i \delta x_i}$$

where the opacity, $K_i(\rho, T)$, and density, ρ_i depend on the local $n_e(x_i, t_n)$ and $T_e(x_i, t_n)$, and δx_i is the dimension on the grid. The total transmission for the entire absorption pulse is a mean defined by

$$\tau = \frac{\int_n F(t)\tau(t) dt}{\int_n F(t) dt}$$

where $F(t)$ is the time envelope of the probe laser.

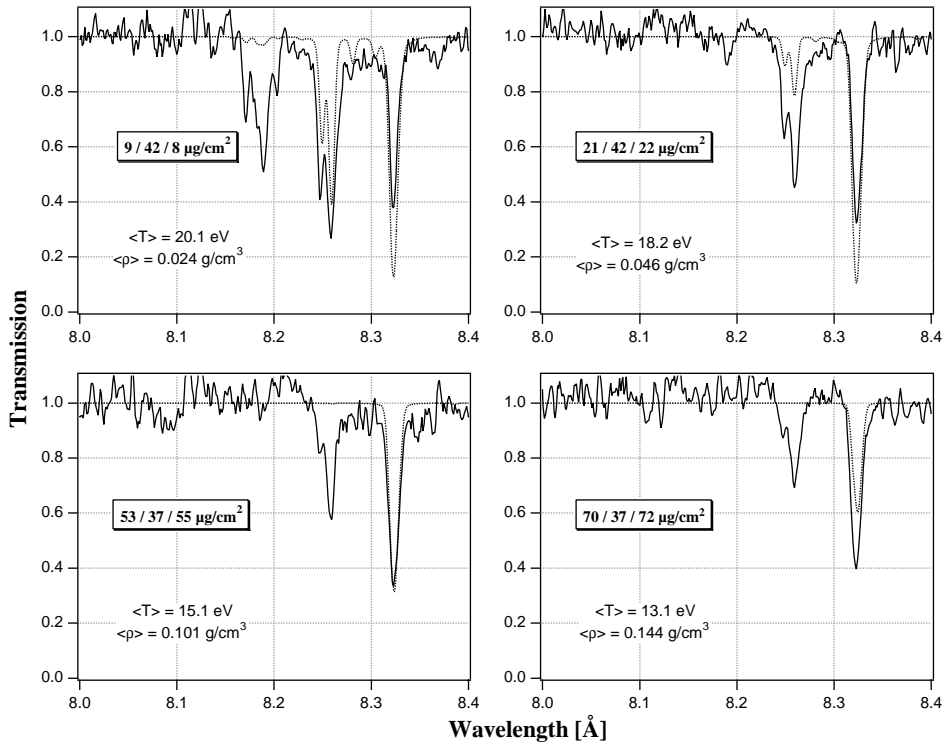


Fig. 8. Comparison of HULLAC modeling for averaged values of the density and temperature, with the aluminum 1s–2p transmission spectra measured for a $40 \mu\text{m}/\text{cm}^2$ Al sample and different carbon thicknesses, as indicated. The measurement is delayed by 500 ps versus the heating pulse. Plain line: experiment; dotted line: simulation.

The comparisons obtained with this method for the different experimental conditions are shown in Fig. 6. The quality of the agreement is obvious. The decrease of ionization ($\langle Z \rangle$ changes from 5 to 4) with increasing tamper thickness is very well reproduced. This variation is explained partly by the increase of the density, but also by the 5 eV decrease of the temperature shown in Fig. 5.

For the cases with other backlight delays shown in Fig. 7, the agreement is not as good as for data obtained for a 500 ps delay. For the 200 and 900 ps delays, the experiment gives a slightly higher ionization state than the simulation. The strong early time variations of the plasma parameters (see Fig. 2) may explain the inability to reproduce the data for a delay of 200 ps. Thus, the time discretization into 10 steps may be too coarse for this rapidly evolving plasma phase. For the 900 ps delay case, where the disagreement is the strongest, ionization freezing due to time-dependent evolution of the populations may occur. We checked this possibility by post-processing the hydrocode data with the atomic time-dependent (TD) code FLY [17]. It shows that LTE and TD results, shown in Fig. 9, are very close inside the sample, but TD ionization stays higher for the hotter part of the Al sample. Indeed, one can see in Fig. 9 that $\langle Z \rangle = 5.6$ instead of $\langle Z \rangle = 5.2$ at LTE, for time = 1500 ps, i.e., 900 ps after the heating pulse maximum. This can explain most of the disagreement at the latest time. The shock of the gold foil that can heat the sample plasma may also be a contributing factor. For a 900 ps delay, the collision happens before the end of the backlighter pulse. Interestingly, the

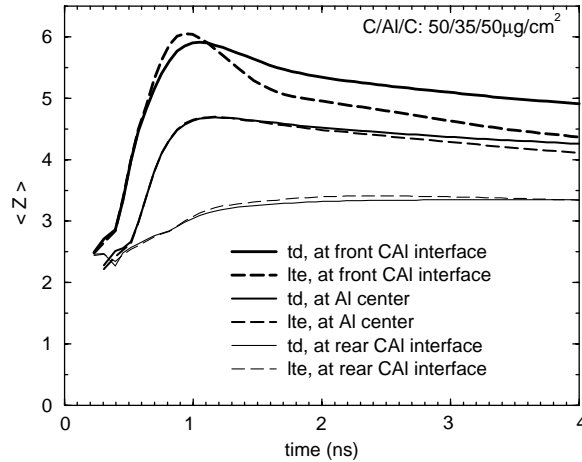


Fig. 9. Average ionization obtained with the code MULTI post-processed with the collisional radiative FLY model, obtained for the sample indicated, and a view factor of 10%. Plain curves are calculated with the time-dependent model, for the cell at the front, at the middle and at the rear of the Al sample. Dashed lines are obtained when LTE is imposed.

Table 2

Ion populations for $T = 13.42$ eV, $\rho = 0.027$ g/cm³, using HULLAC plus Saha equation formalism (col. 2), and using the superconfiguration approach (col. 3)

Z	HULLAC+Saha equation	SCO
1	9.8×10^{-4}	9.551×10^{-3}
2	8.618×10^{-2}	0.1797
3	0.8277	0.6419
4	8.48×10^{-2}	0.1673
5	3.05×10^{-4}	1.613×10^{-3}
$\langle Z \rangle$	2.997	2.972

FLY simulations give an average ionization value close to the data obtained from the experiment, and shown in Table 1.

A few calculations have been performed with the SCO code. The populations of the various ion species obtained with SCO and HULLAC are detailed in Table 2 for $T_e = 13.4$ eV and $\rho = 0.027$ g/cm³. It appears that the ion distribution is roughly the same in both approaches. A closer inspection of the results demonstrates that the SCO approach slightly favors the high charge states. This is probably due to the fact that because of the nuclear screening, the charge experienced by the bound electrons is slightly smaller in the SCO approach than in HULLAC. As a rule, the SCO model provides a broader charge distribution. This could have a small but measurable effect on the transmission spectra presented in this paper. To have a full comparison, hydrocode simulations should be post-processed with SCO and this will be performed for future experiments where aluminum will be replaced by nickel.

7. Conclusions and future plans

Measurements of the transmission of Al samples at high density ($0.02\text{--}0.15\text{ g/cm}^3$) and temperatures in the range 13–20 eV have been performed using thick C tampers. This has been possible due to the high transmission of carbon at the energy of the XUV energies used to heat the sample. Experimental transmission was compared to data calculated by post-processing the hydrocode simulation results with the atomic code HULLAC where the time and space variations of the plasma parameters were taken into account. A substantial decrease of the Al ionization was measured for the thicker carbon tampers. The technique used here will be applied to analyze the transmission of high-density nickel samples in the near future. In this case, coupling the SCO code with radiative hydrodynamic simulations will be necessary.

Future facilities with improved laser performance will give higher and more isotropic radiation fluxes, yielding higher sample temperatures and densities. Coupling such high-energy lasers with a very short pulse backlighter (in the 10 ps duration range) will provide much better time resolution for the opacity measurements. Short backlighter pulses should allow one to probe the heated plasma very early. This should dramatically increase the range of plasma parameters accessible in these laser-driven opacity measurements.

Acknowledgements

We thank the LULI staff for technical assistance. Thin foils were made in University of Munich and Laboratoire des Cibles in Institut de Physique Nucléaire in Orsay University. This work was supported by the European Union through the contract no. FMGECT950044 of the Large-Scale Facility TMR program.

References

- [1] Turck-Chièze S, Basu S, Brun AS, Christensen-Dalsgaard J, Eff-Darwich A, Lopes I, Pérez-Hernandez F, Berthomieu G, Provost J, Ulrich RK, Baudin F, Boumier P, Charra J, Gabriel AH, Garcia RA, Grec G, Renaud C, Robillot JM, Roca Cortès T. First view of the solar core from GOLF acoustic modes. *Sol Phys* 1997;175:247–65.
- [2] Behar E, Sako M, Kahn SM. Soft X-ray absorption by Fe⁰⁺ to Fe in active galactic nuclei. *Astrophys J* 2001;563:497–504.
- [3] Chenais-Popovics C. Astrophysics in laboratory: opacity measurements. *Laser Part Beams* 2002;20:291–8.
- [4] Chenais-Popovics C, Fajardo M, Thais F, Gilleron F, Gauthier J-C, Eidmann K, Fölsner W, Blenski T, Perrot F, Bauche-Arnoult C, Bachelier A, Bauche J. Absorption measurements of radiatively heated multi-layered Al/Ni foils. *JQSRT* 2001;71:249–56.
- [5] Bar-Shalom A, Klapisch M, Oreg J. An integrated computer package for atomic processes in plasmas. *JQSRT* 2001;71:169–88.
- [6] Perrot F, Blenski T, Grimaldi A. Calculation of plasma transmission spectra using the superconfiguration method with orbital relaxation effects. *JQSRT* 1997;58:845–50.
- [7] Blenski T, Grimaldi A, Perrot F. A superconfiguration code based on the local density approximation. *JQSRT* 2000;65:91–100.
- [8] Ramis R, Schmalz R, Meyer-ter-Vehn J. *Comput Phys Commun* 1988;49:475–505.
- [9] Mirone A, Gauthier J-C, Gilleron F, Chenais-Popovics C. Non-LTE opacity calculations with n-l splitting for radiative hydrodynamic codes. *JQSRT* 1997;58:791–802.

- [10] Gilleron F. Étude du transfert radiatif et de l'opacité d'un plasma créé par rayonnement X. PhD thesis, École Polytechnique, 2000.
- [11] Chenais-Popovics C, Gilleron F, Fajardo M, Merdji H, Missalla T, Gauthier J-C, Renaudin P, Gary S, Bruneau J, Perrot F, Blenski T, Fölsner W, Eidmann K. Radiative heating of B, Al and Ni thin foils at 15–25 eV temperatures. *JQSRT* 2000;65:117–33.
- [12] Koenig E. Fonctions d'onde atomiques relativistes dans l'approximation du champ central. Application au Cs I. *Physica* 1972;62:393–408.
- [13] Klapish M, Schwob JL, Fraenkel BS, Oreg J. The 1s–3p K β -like X-ray spectrum of highly ionized iron. *J Opt Soc Am* 1977;67:148.
- [14] Bar-Shalom A, Oreg J, Goldstein WH, Shvarts D, Zigler A. Super-transition-arrays: a model for the spectral analysis of hot, dense plasma. *Phys Rev A* 1989;40:3183–93.
- [15] Pain J-C, Blenski T. *JQSRT*, in preparation.
- [16] Pain J-C. Sur la physique atomique des ions dans les plasmas en présence de l'écrantage. PhD thesis, Université Paris XI Orsay, 2002.
- [17] Chung HK. *JQSRT*, in preparation.
Lee RW, Whitten BL, Strout III RE. SPECTRA—a model for K-shell spectroscopy. *JQSRT* 1984;32:91.